TUDelft

Delft University of Technology

Liquid exfoliation of multilayer graphene in sheared solvents

A molecular dynamics investigation

Gravelle, Simon; Kamal, Catherine ; Botto, Lorenzo

Important note
To cite this publication, please use the final published version (if applicable).
Please check the document version above.

Liquid exfoliation of multilayer graphene in sheared solvents: A molecular dynamics investigation

Simon Gravelle (iD), Catherine Kamal (iD), and Lorenzo Botto (iD)

COLLECTIONS

Paper published as part of the special topic on 2D Materials
Note: This paper is part of the JCP Special Topic on 2D Materials.

Liquid exfoliation of multilayer graphene in sheared solvents: A molecular dynamics investigation

Simon Gravelle,[1] (iD) Catherine Kamal,[1] (iD) and Lorenzo Botto[1,2,a)] (iD)

AFFILIATIONS

[1] School of Engineering and Material Science, Queen Mary University of London, London, United Kingdom
[2] Process and Energy Department, 3ME Faculty of Mechanical, Maritime and Materials Engineering, TU Delft, Delft, The Netherlands

Note: This paper is part of the JCP Special Topic on 2D Materials.
[a)] Author to whom correspondence should be addressed: l.botto@tudelft.nl

ABSTRACT

Liquid-phase exfoliation, the use of a sheared liquid to delaminate graphite into few-layer graphene, is a promising technique for the large-scale production of graphene. However, the microscale and nanoscale fluid-structure processes controlling the exfoliation are not fully understood. Here, we perform non-equilibrium molecular dynamics simulations of a defect-free graphite nanoplatelet suspended in a shear flow and measure the critical shear rate $\dot{\gamma}_c$ needed for the exfoliation to occur. We compare $\dot{\gamma}_c$ for different solvents, including water and N-methyl-pyrrolidone, and nanoplatelets of different lengths. Using a theoretical model based on a balance between the work done by viscous shearing forces and the change in interfacial energies upon layer sliding, we are able to predict the critical shear rates $\dot{\gamma}_c$ measured in simulations. We find that an accurate prediction of the exfoliation of short graphite nanoplatelets is possible only if both hydrodynamic slip and the fluid forces on the graphene edges are considered and if an accurate value of the solid–liquid surface energy is used. The commonly used "geometric-mean" approximation for the solid–liquid energy leads to grossly incorrect predictions.

Published under license by AIP Publishing. https://doi.org/10.1063/1.5141515

I. INTRODUCTION

Two-dimensional materials are made of a single layer of atoms and show physical properties not accessible with bulk materials.[1,2] In particular, charge and heat transport confined to a plane display unusual behavior.[3] Among the family of two-dimensional materials, graphene is considered the thinnest and strongest material ever measured.[4] Graphene possesses outstanding electrical, transport, and thermal properties, and is an appealing candidate for numerous applications in fields such as electronics,[5] energy generation and storage,[6] or biomedicine.[7] However, the fabrication of single or few-layer graphene at the industrial scale remains a challenge.

Liquid-phase exfoliation is a promising technique for the large-scale production of graphene.[8] It consists of dispersing microparticles of graphite in a liquid and forcing the separation of the particles into fewer-layer graphene by using a large shear flow.[9–11] For rigid platelets, the exfoliation is expected to occur if the work of the hydrodynamic forces applied by the liquid on the layered particles is larger than the change in energy associated with the dissociation of the layers.[12,13] The objective of the present article is to quantify this statement using molecular dynamics (MD).

The change in energy associated with the separation of two layers in a liquid can be estimated following a model originally proposed by Chen *et al.*[12] and later improved by Paton *et al.*[13] One considers a bilayer nanoplatelet of length L and width w immersed in a liquid. The total surface energy of the bilayer particle before exfoliation is

$$E_{\text{init}} = -Lw(\mathcal{E}_{ss} + \mathcal{E}_{\ell\ell} + 2\mathcal{E}_{\ell s}), \tag{1}$$

where $\mathcal{E}_{ss}$, $\mathcal{E}_{\ell\ell}$, and $\mathcal{E}_{\ell s}$ are the solid–solid, liquid–liquid, and liquid–solid surface energy densities, respectively (Fig. 1). After exfoliation, the total surface energy of the separated particles is (see Fig. 1)

$$E_{\text{final}} = -4Lw\mathcal{E}_{\ell s}. \tag{2}$$

The total change in energy $\Delta E = E_{\text{final}} - E_{\text{init}}$ associated with the particle exfoliation is, thus,

$$\Delta E = Lw(\mathcal{E}_{ss} + \mathcal{E}_{\ell\ell} - 2\mathcal{E}_{\ell s}). \tag{3}$$

Since $\mathcal{E}_{\ell s}$ is not known in general, the geometric mean approximation $\mathcal{E}_{\ell s} = \sqrt{\mathcal{E}_{\ell\ell}\mathcal{E}_{ss}}$ connecting the solid–liquid to the liquid–liquid and solid–solid surface energies is commonly used, resulting in

$$\Delta E = Lw\left(\sqrt{\mathcal{E}_{\ell\ell}} - \sqrt{\mathcal{E}_{ss}}\right)^2. \tag{4}$$

Exfoliation is expected if the work done by the tangential hydrodynamic force $\mathcal{W}_{\text{hyd}}$ applied by the shearing liquid on the particle is larger than ΔE. Assuming the no-slip boundary condition and ignoring contributions from the edges of the platelet, the tangential hydrodynamic force driving the relative sliding of the top and bottom layers is $F_{\text{hyd}} \approx \eta\dot{\gamma}wL$, where η is the fluid viscosity and $\dot{\gamma}$ is the shear rate applied to the fluid.[15] The total work required for the hydrodynamic force to separate one layer from the other in a sliding deformation can be estimated as

$$\mathcal{W}_{\text{hyd}} = F_{\text{hyd}}L \approx \eta\dot{\gamma}wL^2. \tag{5}$$

By equating Eqs. (4) and (5), the following expression for the critical shear rate value $\dot{\gamma}_c$ above which exfoliation is expected is obtained:

$$\dot{\gamma}_c \approx \frac{1}{\eta L}\left(\sqrt{\mathcal{E}_{\ell\ell}} - \sqrt{\mathcal{E}_{ss}}\right)^2. \tag{6}$$

Equation (6) suggests that some fluids are a better choice than others for liquid-phase exfoliation because their surface energy is close to the surface energy of graphene. Indeed, it has been shown experimentally that exfoliation was the most efficient when performed with solvents such as N-methyl-pyrrolidone (NMP) and dimethylformamide (DMF),[9,10,16] whose surface energies are $\mathcal{E}_{\ell\ell} \sim 68$ mJ/m^2. Therefore, Eq. (6) suggests that the surface energy of graphene is $\mathcal{E}_{ss} \sim 68$ mJ/m^2, a value that is reasonably close to that obtained with contact angle measurements.[17] However, a broad range of values for the surface energy of graphene has been reported. For instance, a direct measurement of the surface energy using a
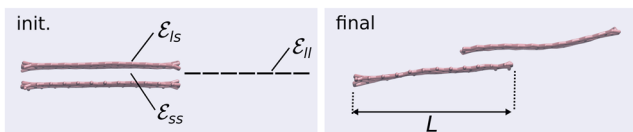
surface force apparatus[18] gave $\mathcal{E}_{ss} = 115 \pm 4$ mJ/m^2. If we use this value in Eq. (6), we obtain $\dot{\gamma}_c = 4 \cdot 10^6$ s^{-1} for micrometric particles in the NMP fluid, which does not compare well with the experimental values of $\dot{\gamma}_c \approx 10^4$ s^{-1}.[13] In addition, some solvents with surface energy $\mathcal{E}_{\ell\ell} \sim 68$ mJ/m^2 are known to be a poor choice for graphene exfoliation.[10] Therefore, the high efficiency of NMP and DMF to exfoliate graphite nanoparticles remains a mystery, suggesting that the accuracy of Eq. (6) has to be reconsidered.

It has been proposed that the Hansen solubility parameter, which accounts for dispersive, polar, and hydrogen-bonding components of the cohesive energy density of a material, is a much better indicator of the quality of a solvent for the exfoliation of graphene.[10,19] However, the Hansen solubility parameter also leads to contradictory results as it suggests that ideal fluids for graphene dispersion are fluids with non-zero value of polar and hydrogen-bonding parameters, even though graphene is nonpolar.[19]

In addition to experiments, molecular dynamics simulations have been used to evaluate the respective exfoliation efficiency of different fluids. Most authors have measured the potential of mean force (PMF) associated with the peeling of a layer or the detachment of parallel rigid layers.[20–23] When performed in a liquid, such a measurement gives precious information on the thermodynamic stability of dispersed graphene and have shown that NMP should have excellent performance for graphene exfoliation, in agreement with experimental data.[23] However, PMF measurements are static and do not account for the dynamic effects associated with the exfoliation process.

In this context, we perform non-equilibrium molecular dynamics (MD) simulations of the exfoliation of graphite platelets by different shearing fluids, starting with NMP and water. We record the critical shear rate $\dot{\gamma}_c$ above which exfoliation occurs and compare our results with Eq. (6). Our results emphasize that Eq. (6) is limited in its predictive capability, and we, therefore, propose an alternative to Eq. (6) that accounts for, among other effects, hydrodynamic slip. Slip reduces the hydrodynamic stress in the direction parallel to the surface and, therefore, significantly affects the tangential hydrodynamic force applied by the shearing liquid on the particle.

II. RESULT

We perform MD simulations of a freely suspended graphite particle in a shear flow using the Large-scale Atomic/Molecular Massively Parallel Simulator (LAMMPS).[24] The initial configuration consists of a stack of N graphene layers immersed in a liquid, with N between 2 and 6. Rigid walls are used to enclose the fluid in the $\vec{e}_y$ direction (Fig. 2). Periodic boundary conditions are used in the three orthogonal directions. The effective thickness of the platelet in the $\vec{e}_y$ direction is H, its length in the $\vec{e}_x$ direction is L, and the span-wise dimension of the computational domain in the $\vec{e}_z$ direction is w. The simulation box is equal to $3 \times L$ in the $\vec{e}_x$ direction, 2 nm in the $\vec{e}_y$ direction, and the distance between the rigid walls is $H_w \approx 14$ nm. Based on a preliminary convergence study, H_w and the dimensions of the computational box were chosen large enough to avoid finite-size effects. We use the Adaptive Intermolecular Reactive Empirical Bond Order (AIREBO) force field for graphene.[25] The fluid consists of a number N_f of water molecules or N-Methyl-2-pyrrolidone (NMP) molecules. We use the TIP4P/2005 model for water[26] and

FIG. 1. Schematic of a bilayer nanoparticle of length L in a liquid before exfoliation (initial), with the three different surface energy terms, and the same nanoparticle after exfoliation into two single-layer platelets (final).
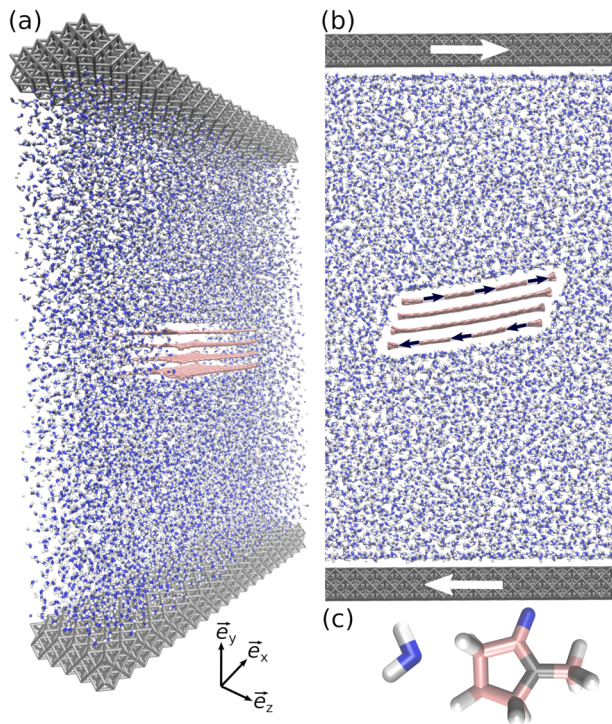
FIG. 2. [(a) and (b)] Molecular dynamics snapshots of a four-layer graphite nanoparticle prior to exfoliation in water.[14] The particle has size dimension L in the $\vec{e}_x$ direction and height H in the $\vec{e}_y$ direction. The third dimension in the $\vec{e}_z$ direction is w. Two moving walls impose a linear shear flow profile on the liquid. The black arrows indicate qualitatively the direction of the tangential hydrodynamic force applied to the top and bottom layers on the nanoparticle. (c) Water (left) and NMP (right) molecules.

FIG. 3. Exfoliation of graphite in water. (a) Shear rate $\dot{\gamma}$ as a function of the nanoplatelet length L for an initial number of layers $N = 4$. The red disks correspond to the simulations for which exfoliation was observed, and blue squares correspond to the simulations for which exfoliation was not observed. (b) Shear rate $\dot{\gamma}$ as a function of N for $L = 2.8$ nm. (c) Critical shear rate $\dot{\gamma}_c$ above which exfoliation occurs as a function of L as extracted from MD simulation (symbols). The black dotted line is Eq. (6), the black dashed line is Eq. (11), and the blue full line is Eq. (12) (see text for details). (d) Critical shear rate $\dot{\gamma}_c$ as a function of the initial number of layers.

the all-atom Gromos force field for NMP.[27] Carbon-fluid interaction parameters are calculated using the Lorentz–Berthelot mixing rule. The initial molecular structure of NMP is extracted from the automated topology builder.[28] A shear flow of strength $\dot{\gamma}$ is produced by the relative translation of the two parallel walls in the $\vec{e}_x$ direction, with respective velocities $U/2$ and $-U/2$. The two walls also impose atmospheric pressure on the fluid. Fluid molecules are maintained at a constant temperature of $T = 300$ K using a Nosé–Hoover temperature thermostat[29,30] applied only to the degrees of freedom in the directions normal to the flow, $\vec{e}_y$ and $\vec{e}_z$.

During the initial stage of the simulation, the walls are allowed to move in the $\vec{e}_y$ direction to impose a constant pressure of 1 atm on the fluid, and the graphene layers are maintained immobile. After 50 ps, the graphene particle is allowed to freely translate and rotate using constant NVE integration, and the velocities of the walls in the $\vec{e}_x$ direction are set equal to $U/2$ and $-U/2$, respectively, with $U = H_w \dot{\gamma}$. Each simulation is performed for a duration of 1 ns in addition to the 50 ps of the initial stage. Simulations are performed at a fixed shear rate $\dot{\gamma}$, for a given number of layers N and length L of each layer.

The state of the graphite particle is controlled during the simulation, and two recurring situations are identified: (i) sliding of the layers does not occur [blue squares in Figs. 3(a) and 3(b)] or
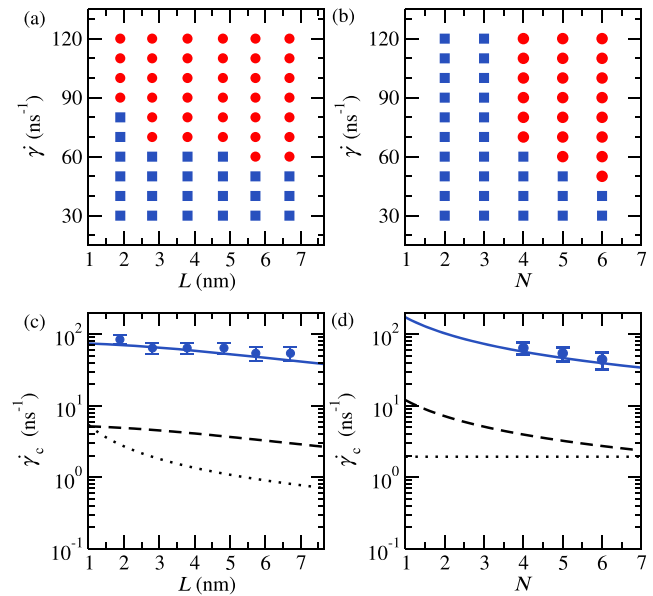
(ii) the platelet is exfoliated into a variable number of fewer-layer platelets [red disks in Figs. 3(a) and 3(b)]. We associate the transition between the unaltered (blue) phase and the exfoliated (red) phase with a critical shear rate $\dot{\gamma}_c$; $\dot{\gamma}_c$ decreases with the nanoplatelet length, as well as with the initial number of nanoplatelet N [Figs. 3(c) and 3(d)]. In the case of water fluid, for an initial number of layers $N \leq 3$, no exfoliation is observed, even for $\dot{\gamma}$ as high as 120 ns^{-1}.

Similar simulations are performed using NMP [Figs. 4(a) and 4(b)]. For NMP and a given number of layers N, the critical shear rate $\dot{\gamma}_c$ above which exfoliation is observed is typically one order of magnitude lower than in water [Figs. 4(c) and 4(d)], a difference that cannot be explained by the difference in viscosity of the two fluids ($\eta = 0.855$ mPa s for TIP4P/2005 water at 300 K[31] and $\eta = 1.6$ mPa s for NMP[32]). Unlike for water, for which the critical shear rate $\dot{\gamma}_c$ is not visible for $N = 2$ and 3 (Fig. 3), a value for $\dot{\gamma}_c$ has been obtained for any value of N and L in the case of a NMP fluid (Fig. 4).

The critical shear rate $\dot{\gamma}_c$ obtained using MD can be compared with the prediction of Eq. (6). To do so, both solid–solid $\mathcal{E}_{ss}$ and liquid–liquid $\mathcal{E}_{\ell\ell}$ surface energies are needed. The surface energy of graphene corresponds to half the work required to separate two initially bounded layers.[33] We find $\mathcal{E}_{ss} = 147$ mJ/m^2 for the AIREBO force field at zero temperature (supplementary material). The liquid–liquid surface energy follows from the surface tension
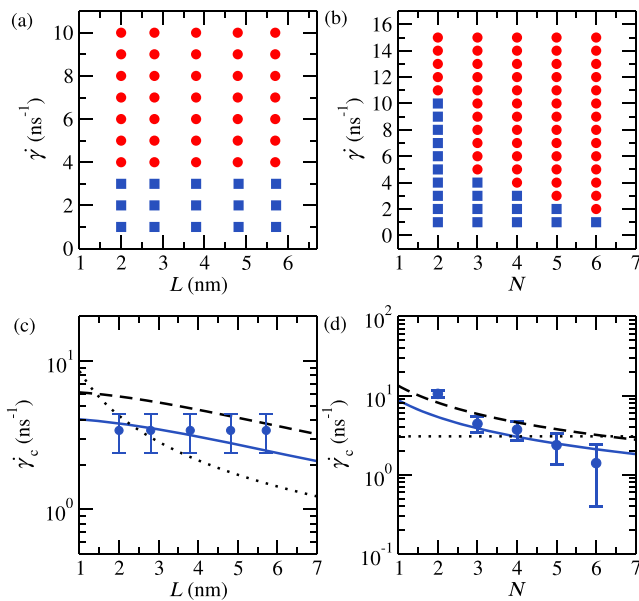
FIG. 4. Exfoliation of graphite in NMP. (a) Shear rate $\dot{\gamma}$ as a function of the nanoplatelet length L for an initial number of platelets $N = 4$. The red disks correspond to the simulations for which exfoliation was observed, and blue squares correspond to the simulations for which exfoliation was not observed. (b) Shear rate $\dot{\gamma}$ as a function of N and fixed $L = 2.8$ nm. (c) Critical shear rate $\dot{\gamma}_c$ above which exfoliation occurs as a function of L as extracted from MD simulation (symbols). The black dotted line is Eq. (6), the black dashed line is Eq. (11), and the blue full line is Eq. (12) (see text for details). (d) Critical shear rate $\dot{\gamma}_c$ as a function of the initial number of layers.

σ as $\mathcal{E}_{\ell\ell} = \sigma + TS$, where S is the entropy.[34] Using the universal value for the entropy $S \sim 0.1$ mJ m^{-2} K^{-1} [13] and using literature values for the surface tension of water and NMP, one gets $\mathcal{E}_{\ell\ell} = 99.5$ mJ/m^2 for water and $\mathcal{E}_{\ell\ell} = 71$ mJ/m^2 for NMP at $T = 300$ K.[35,36] Results show that Eq. (6) fails to predict $\dot{\gamma}_c$, particularly in the case of water [dotted lines in Figs. 3(c), 3(d), 4(c), and 4(d)]. In addition, Eq. (6) predicts a functional form $\dot{\gamma}_c \propto L^{-1}$ that is in disagreement with the MD results and fails to capture the variation of $\dot{\gamma}_c$ with the initial number of layers N.

III. MODEL FOR THE EXFOLIATION OF NANOPLATELET

To improve the accuracy of Eq. (6), one first needs to improve the expression for the work of the hydrodynamic force [Eq. (5)]. For nanomaterials with a smooth surface such as graphene and for most solvents, the classical no-slip boundary condition is often inaccurate and should be replaced by a partial slip boundary condition.[37] The hydrodynamic slip at the solid–liquid interface can be characterized by a Navier slip length λ, which is the distance within the solid at which the relative solid–fluid velocity extrapolates to zero.[38,39] In order to quantify the effect of slip on the hydrodynamic force, we consider the traction vector $\boldsymbol{f} = \boldsymbol{T} \cdot \boldsymbol{n}$, where $\boldsymbol{T}$ is the fluid stress tensor and $\boldsymbol{n}$ is the normal to the surface. The traction can be calculated exactly by solving a boundary integral equation.[40] For a thin particle aligned in the direction of the undisturbed shear flow (at high shear rates, an elongated particle spends most of the time aligned

in the flow direction[15,41]), the traction can be estimated analytically by expanding the boundary integral equation to leading order in $H/L \ll 1$.[15,41] Accounting for a Navier slip boundary condition,[40] this asymptotic analysis yields the following leading-order expression for the hydrodynamic tangential traction,[41] valid far from the edges:

$$f_x \equiv \boldsymbol{f} \cdot \boldsymbol{e}_x = \frac{\dot{\gamma}\eta}{1 + 8\lambda/(\pi L)}. \quad (7)$$

Because f_x is uniform, the leading-order contribution to F_{hyd} from the flat surface of the graphene particle is

$$\int_{A_t} f_x \, dS \approx \frac{\dot{\gamma}\eta w L}{1 + 8\lambda/(\pi L)}, \quad (8)$$

where $|A_t| \approx wL$. Since the slip length for graphene in water is typically $\lambda \approx 10$ nm,[42–44] slip reduces the hydrodynamic force applied by the fluid on the platelet by a factor $1 + 8\lambda/(\pi L) \approx 7$, assuming a length of $L = 4$ nm.

In addition to the force due to shearing of the flat surfaces, an additional hydrodynamic contribution is due to the force on the edges of the platelet.[15] For a nanometric platelet, these edge effects can even be dominant, in particular, for a platelet with a large slip length.[41] Because stresses in Stokes flow scale proportionally to $\eta\dot{\gamma}$, and the edge hydrodynamics is controlled by the thickness H, the edge force is expected to scale as $F_{\text{hyd}}^e \sim \dot{\gamma}\eta wH$. Using the fact that $H \simeq Nd$, where $d \approx 3.4$ Å is the inter-layer distance, we can write

$$F_{\text{hyd}}^e \approx \dot{\gamma}\eta wcNd. \quad (9)$$

Our simulation data from both the boundary integral method (BIM) and MD simulations indeed support the scaling of Eq. (9), suggesting $c \simeq 1.5$ [with some dispersion; actual values range between 1 and 2, suggesting a weak dependence on N and λ; see Figs. 5(a) and 5(b) and Fig. S1 of the supplementary material]. Including the edge force, the total hydrodynamic force driving the inter-layer sliding is
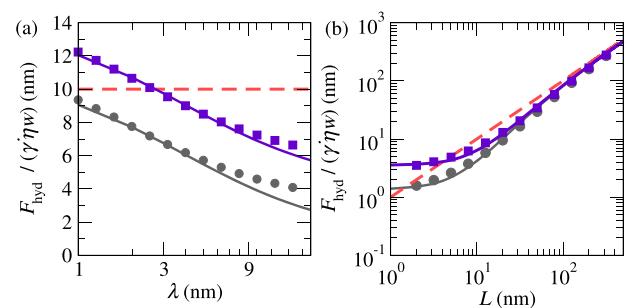

FIG. 5. (a) Continuum calculations of the lateral hydrodynamic force applied by the liquid on the top platelet with length $L = 10$ nm, $N = 2$ (gray disks), $N = 8$ (purple squares), as a function of the slip length λ. Calculations are made using the boundary integral method (BIM, supplementary material). Full lines are Eq. (10) with $c \approx 1.5$, and the red dashed line is the no-slip, no edge effect approximation, $F_{\text{hyd}}/(\dot{\gamma}\eta w) = L$. (b) BIM calculations for a platelet with $\lambda = 10$ nm, $N = 2$ (gray disks), $N = 8$ (purple squares), as a function of L. Full lines are Eq. (10) with, respectively, $c = 1.8$ ($N = 2$) and $c = 1.2$ ($N = 8$), and the red dashed line is the no-slip, no edge effect approximation.

$$F_{\text{hyd}} \approx \dot{\gamma}\eta w \left(\frac{L}{1 + 8\lambda/(\pi L)} + cNd \right). \tag{10}$$

For $N = 4$, $L = 4$ nm, and $\lambda = 10$ nm, one gets that the contribution from the edges [term containing cNd in Eq. (10)] is more than five times larger than the contribution from the flat surfaces [term containing λ in Eq. (10)]. Not accounting for the corrections in Eq. (10) can lead to large errors, particularly for $L < 20$ nm [Fig. 5(b)].

Now, inserting Eq. (10) into the expression for the work [Eq. (5)] and balancing Eqs. (4) and (5), one gets a critical shear rate

$$\dot{\gamma}_c \approx \frac{1}{\eta} \frac{\left(\sqrt{\mathcal{E}_{\ell\ell}} - \sqrt{\mathcal{E}_{ss}} \right)^2}{L/(1 + 8\lambda/(\pi L)) + cNd}. \tag{11}$$

Unlike Eq. (6), Eq. (11) appears to have the same trend as the MD data, for changes in L or N (dashed lines in Figs. 3 and 4). Here, we used our independent measurements for the slip length, $\lambda = 60$ nm for water and $\lambda = 12$ nm for NMP (supplementary material). However, the predictions from Eq. (11) are still in quantitative disagreement with the MD measurements, suggesting that the remaining problem is in the estimation of ΔE.

Equation (4) has been obtained using the geometric mixing rule. However, this semi-empirical rule is not accurate in general for predicting solid–liquid surface energy, in particular, for fluids with a polar contribution.[45] To prove this, instead of using the mixing rule, we retain all three energy terms and evaluate ΔE from Eq. (3), leading to

$$\dot{\gamma}_c \approx \frac{1}{\eta} \frac{\mathcal{E}_{\ell\ell} + \mathcal{E}_{ss} - 2\mathcal{E}_{\ell s}}{L/(1 + 8\lambda/(\pi L)) + cNd}. \tag{12}$$

The agreement between Eq. (12) and MD is excellent using $c \approx 1$, $\mathcal{E}_{\ell s} = 90$ mJ/m^2 for water and $\mathcal{E}_{\ell s} = 105$ mJ/m^2 for NMP. These surface energy density values are very close to those we obtained by performing independent measurements of $\mathcal{E}_{\ell s}$, obtained by measuring the difference between longitudinal and transverse pressures near a fluid–solid or fluid–vapor interface.[46–48] We found $\mathcal{E}_{\ell s} = 93 \pm 4$ mJ/m^2 for water–graphene and $\mathcal{E}_{\ell s} = 107 \pm 5$ mJ/m^2 for NMP–graphene (supplementary material).

To test further the general applicability to different solvents of Eq. (12), we performed simulations using four additional liquids: ethanol, benzene, DMF, and toluene [Fig. 6(a)]. These solvents have been selected because together with water and NMP, they offer a broad range of surface energy values (Table S2, supplementary material), and for their low viscosity (≤ 1.1 mPa s). Higher viscosity solvents such as ionic liquid or polymer exhibit non-Newtonian behavior and/or are made of molecules that can be comparable in size or larger than the nanoplatelet graphene studied here. These characteristics are expected to affect the exfoliation behavior through a modification of the hydrodynamic force applied by the solvent on the particle, and so, we limit our study to low-viscosity solvents made of relatively small molecules. For a graphite particle of length $L = 3.6$ nm and initial layer number $N = 4$, we have extracted the critical shear rate $\dot{\gamma}_c$ for each solvent. We report the critical shear stress values $\eta\dot{\gamma}_c$ for each fluid as a function of $(\mathcal{E}_{\ell\ell} + \mathcal{E}_{ss} - 2\mathcal{E}_{\ell s})/(L/(1 + 8\lambda/(\pi L)) + cNd)$, where the surface energy
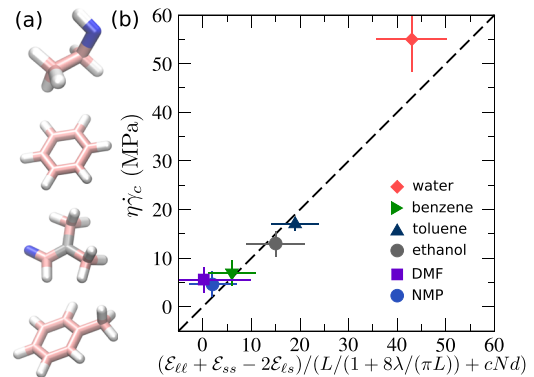

FIG. 6. (a) From top to bottom: ethanol, benzene, DMF, and toluene molecules. (b) Critical shear stress $\eta\dot{\gamma}_c$ as measured from MD as a function of the normalized energy difference $(\mathcal{E}_{\ell\ell} + \mathcal{E}_{ss} - 2\mathcal{E}_{\ell s})/(L/(1 + 8\lambda/(\pi L)) + cNd)$ [expressed in mJ/(m^2/nm)] with $c \approx 1$ (see the text for details). The dashed line is a $y = x$ guide for the eye.

$\mathcal{E}_{\ell s}$ and slip length have been measured independently for each fluid. MD results for the seven different fluids show a good agreement with Eq. (12) [Fig. 6(b)].

IV. DISCUSSION

In this article, we used non-equilibrium MD to simulate the exfoliation of defect-free graphite nanoplatelets. We measured the critical shear rate $\dot{\gamma}_c$ above which exfoliation occurs using different solvents, with a particular focus on comparing NMP, typically considered an optimal solvent for the exfoliation of pure graphene, and water, typically considered not a good solvent. We compared the MD results with a simple theoretical model based on a balance between the work done by hydrodynamic forces and the change in interfacial energy associated with the separation of the layers. We find a good agreement between the model and MD provided that (i) the hydrodynamic force accounts for slip at the solid–fluid interface, (ii) the hydrodynamic force accounts for additional edge-related contributions, and (iii) the full energy difference associated with the separation of the layers is accounted for.

Since the validity of Eq. (12) has been demonstrated by comparison with MD, we can use it to predict the critical shear rate $\dot{\gamma}_c$ for a platelet with more realistic dimensions and compare the outcome with experimental data. Using microfluidization, Karagiannidis *et al.*[49] have reported the exfoliation of graphite in aqueous solution (sodium deoxycholate and de-ionized water) for shear rates above $\dot{\gamma}_c \sim 10^8$ s^{-1}. Assuming $L = 1$ μm, the mean flake size reported by Karagiannidis *et al.*, as well as $N = 10$ and $\lambda = 10$ nm, a typical experimental slip length value for graphene,[42,43] we have $\lambda/L \ll 1$ and $cNd/L \ll 1$ [Fig. 5 (b)] such that

$$\dot{\gamma}_c \approx \frac{1}{\eta L}(\mathcal{E}_{\ell\ell} + \mathcal{E}_{ss} - 2\mathcal{E}_{\ell s}). \tag{13}$$

Using the MD's values for $\mathcal{E}_{ss}$ and $\mathcal{E}_{\ell s}$, together with the experimental values for η and $\mathcal{E}_{\ell\ell}$ (Table S2, supplementary material), Eq. (13)

gives $\dot{\gamma}_c = 6 \cdot 10^7 \, \text{s}^{-1}$, which is close to the value of $\dot{\gamma}_c \sim 10^8 \, \text{s}^{-1}$ reported by Karagiannidis et al.[49]

Using a rotating mixer, Paton et al. have reported the exfoliation of graphite in NMP for shear rates above $\dot{\gamma}_c \sim 10^4 \, \text{s}^{-1}$. In such experiments, $\lambda/L \ll 1$ and $cNd/L \ll 1$, so Eq. (13) can again be used to predict the critical shear rate. Using the MD's values for $\mathcal{E}_{ss}$ and $\mathcal{E}_{\ell s}$, together with the experimental values for η and $\mathcal{E}_{\ell\ell}$, Eq. (13) predicts $\dot{\gamma}_c = 4 \cdot 10^6 \, \text{s}^{-1}$, a value that is two orders of magnitude larger than the experimental value.

There are many potential reasons for this discrepancy. One is the thermally induced wrinkling of the sheets, which could play a role in modulating the adhesion forces, particularly in the case of larger sheets. However, experiments with graphene oxide show that these undulations are strongly suppressed under shear.[50] A second explanation for the discrepancy is the possible importance in experiments of bending deformations. Bending deformations are relatively unimportant in our MD simulations because the nanosheets have small lengths and are, therefore, relatively rigid, but the same cannot be said for microsheets and nanosheets having L in the micrometer range. For graphene multilayers where at least one of the layers deforms significantly by bending, the energy balance should include a bending energy term associated with the internal work of deformation of the solid, in addition to external work and adhesion energy terms.[51] A simple dimensional analysis suggests that the most general expression for the critical shear rate is[52]

$$\dot{\gamma}_c \approx \frac{1}{\eta L} \frac{\mathcal{E}_{\ell\ell} + \mathcal{E}_{ss} - 2\mathcal{E}_{\ell s}}{g(\dot{\gamma}\eta L^3/B)}, \qquad (14)$$

where g is a non-dimensional function that accounts for the effect of flexibility on the force resisting exfoliation (e.g., accounting for stress concentration effects in peeling deformations) and B is the bending rigidity of the deforming layer. For $\dot{\gamma}\eta L^3/B \ll 1$ (rigid sheets), g is expected to tend to 1, recovering Eq. (13). However, for $\dot{\gamma}\eta L^3/B \sim 1$ or larger, bending deformations become important, and a stronger dependence of $\dot{\gamma}$ on L emerges.[52,53] The considerations made in this paper regarding the quantification of surface energies and hydrodynamic force contributions, however, remain valid, and the comparison of Eq. (12) with MD is an important stepping stone toward accurate predictive models of exfoliation.

A third reason for the discrepancy between experimental and MD results is the sensitivity of the model parameters. A sensitivity analysis of Eq. (13) can be carried out by first writing

$$\dot{\gamma}_c^o \approx \frac{1}{\eta^o L}(\mathcal{E}_{\ell\ell}^o + \mathcal{E}_{ss}^o - 2\mathcal{E}_{\ell s}^o), \qquad (15)$$

where the superscript "o" refers to the *observed* experimental parameters, and then comparing this expression with Eq. (13), which contained *estimated* parameters (from MD). Assuming that the only uncertainties are in the value of $\mathcal{E}_{\ell s}$ (i.e., $\mathcal{E}_{\ell\ell}^o = \mathcal{E}_{\ell\ell}$, $\mathcal{E}_{ss}^o = \mathcal{E}_{ss}$, and $\eta^o = \eta$), one can write the difference between the observed critical shear rate and the predicted one as

$$\dot{\gamma}_c - \dot{\gamma}_c^o \approx \frac{2}{\eta L}(\mathcal{E}_{\ell s}^o - \mathcal{E}_{\ell s}). \qquad (16)$$

Assuming a 1% difference between $\mathcal{E}_{\ell s}$ and $\mathcal{E}_{\ell s}^o$, and since $\mathcal{E}_{\ell s}^o$ is typically of the order of 100 mJ/m^2, one gets $\dot{\gamma}_c - \dot{\gamma}_c^o$ of the order of $10^6 \, \text{s}^{-1}$ for $L = 1 \, \mu\text{m}$ and $\eta = 1$ mPa s. Since in the case of NMP, $\dot{\gamma}_c^o \approx 10^4 \, \text{s}^{-1}$, an error of only one percent on $\mathcal{E}_{\ell s}$ leads to a difference by two orders of magnitude between the predicted and the observed value of $\dot{\gamma}_c$. This analysis demonstrates the challenge of drawing definite conclusions regarding the validity of the model by comparing it against experiments in which surface energy parameters are not measured independently.

V. CONCLUSION

In this article, we use non-equilibrium MD to simulate the liquid exfoliation of multilayer graphene platelets. Using different solvents, such as NMP and water, we extract the critical shear rate above which exfoliation occurs. We, then, compare the results with a formalism based on a balance between the work done by the shear forces and the energy difference associated with the exfoliation. We find that an accurate prediction of the exfoliation of short graphite nanoplatelets [see Eq. (12)] is possible only if both the hydrodynamic slip and the fluid forces on the graphene edges are considered and if an accurate value of the solid–liquid surface energy is used [see Eq. (3)].

SUPPLEMENTARY MATERIAL

See the supplementary material for (i) energy measurement at solid interfaces, (ii) slip length measurements, (iii) hydrodynamic force measurement, and (iv) parameters for the 6 fluids, and also Figure S1 and Table S2.

ACKNOWLEDGMENTS

REFERENCES

[1]R. Mas-Ballesté, C. Gómez-Navarro, J. Gómez-Herrero, and F. Zamora, "2D materials: To graphene and beyond," Nanoscale **3**, 20–30 (2011).

[2]N. Mounet, M. Gibertini, P. Schwaller, D. Campi, A. Merkys, A. Marrazzo, T. Sohier, I. E. Castelli, A. Cepellotti, G. Pizzi, and N. Marzari, "Two-dimensional materials from high-throughput computational exfoliation of experimentally known compounds," Nat. Nanotechnol. **13**, 246–252 (2018).

[3]S. Z. Butler, S. M. Hollen, L. Cao, Y. Cui, J. A. Gupta, H. R. Gutiérrez, T. F. Heinz, S. S. Hong, J. Huang, A. F. Ismach, E. Johnston-Halperin, M. Kuno, V. V. Plashnitsa, R. D. Robinson, R. S. Ruoff, S. Salahuddin, J. Shan, L. Shi, M. G. Spencer, M. Terrones, W. Windl, and J. E. Goldberger, "Progress, challenges, and opportunities in two-dimensional materials beyond graphene," ACS Nano **7**, 2898–2926 (2013).

[4]A. K. Geim, "Graphene: Status and prospects," Science **324**, 1530–1534 (2010).

[5]P. Avouris and F. Xia, "Graphene applications in electronics and photonics," MRS Bull. **37**, 1225–1234 (2012).

[6]D. A. C. Brownson, D. K. Kampouris, and C. E. Banks, "An overview of graphene in energy production and storage applications," J. Power Sources **196**, 4873–4885 (2011).

[7]C. Chung, Y.-k. Kim, D. Shin, S.-r. Ryoo, B. H. E. E. Hong, and D.-h. Min, "Biomedical applications of graphene and graphene oxide," Acc. Chem. Res. **46**, 2211–2224 (2013).

[8]M. Yi and Z. Shen, "A review on mechanical exfoliation for scalable production of graphene," J. Mater. Chem. A **3**, 11700 (2015).

[9]Y. Hernandez, V. Nicolosi, M. Lotya, F. M. Blighe, Z. Sun, S. De, I. T. Mcgovern, B. Holland, M. Byrne, K. Y. K. Gun'Ko, J. J. Boland, P. Niraj, G. Duesberg, S. Krishnamurthy, R. Goodhue, J. Hutchison, V. Scardaci, A. C. Ferrari, and J. N. Coleman, "High-yield production of graphene by liquid-phase exfoliation of graphite," Nat. Nanotechnol. **3**, 563–568 (2008).

[10]J. N. Coleman, "Liquid exfoliation of defect-free graphene," Acc. Chem. Res. **46**, 14–22 (2013).

[11]M. Yi and Z. Shen, "Kitchen blender for producing high-quality few-layer graphene," Carbon **78**, 622–626 (2014).

[12]X. Chen, J. F. Dobson, and C. L. Raston, "Vortex fluidic exfoliation of graphite and boron nitride," Chem. Commun. **48**, 3703–3705 (2012).

[13]K. R. Paton, E. Varrla, C. Backes, R. J. Smith, U. Khan, A. O'Neill, C. Boland, M. Lotya, O. M. Istrate, P. King, T. Higgins, S. Barwich, P. May, P. Puczkarski, I. Ahmed, M. Moebius, H. Pettersson, E. Long, J. Coelho, S. E. O'Brien, E. K. McGuire, B. M. Sanchez, G. S. Duesberg, N. McEvoy, T. J. Pennycook, C. Downing, A. Crossley, V. Nicolosi, and J. N. Coleman, "Scalable production of large quantities of defect-free few-layer graphene by shear exfoliation in liquids," Nat. Mater. **13**, 624–630 (2014).

[14]W. Humphrey, A. Dalke, and K. Schulten, "VMD: Visual molecular dynamics," J. Mol. Graphics **14**, 33–38 (1996).

[15]V. Singh, D. L. Koch, G. Subramanian, and A. D. Stroock, "Rotational motion of a thin axisymmetric disk in a low Reynolds number linear flow," Phys. Fluids **26**, 033303 (2014).

[16]S. Ravula, S. N. Baker, G. Kamath, and G. A. Baker, "Ionic liquid-assisted exfoliation and dispersion: Stripping graphene and its two-dimensional layered inorganic counterparts of their inhibitions," Nanoscale **7**, 4338–4353 (2015).

[17]S. Wang, Y. Zhang, N. Abidi, and L. Cabrales, "Wettability and surface free energy of graphene films," Langmuir **25**, 11078–11081 (2009).

[18]C. D. van Engers, N. E. A. Cousens, N. Grobert, B. Zappone, and S. Perkin, "Direct measurement of the surface energy of graphene," Nano Lett. **17**, 3815–3821 (2017).

[19]Y. Hernandez, M. Lotya, D. Rickard, S. D. Bergin, and J. N. Coleman, "Measurement of multicomponent solubility parameters for graphene facilitates solvent discovery," Langmuir **26**, 3208–3213 (2010).

[20]X. An, T. Simmons, R. Shah, C. Wolfe, K. M. Lewis, M. Washington, S. K. Nayak, S. Talapatra, and S. Kar, "Stable aqueous dispersions of noncovalently functionalized graphene from graphite and their multifunctional high-performance applications," Nano Lett. **10**, 4295–4301 (2010).

[21]C.-J. Shih, S. Lin, M. S. Strano, and D. Blankschtein, "Understanding the stabilization of liquid-phase-exfoliated graphene in polar solvents: Molecular dynamics simulations and kinetic theory of colloid aggregation," J. Am. Chem. Soc. **132**, 14638–14648 (2010).

[22]V. Sresht, A. A. Pádua, and D. Blankschtein, "Liquid-phase exfoliation of phosphorene: Design rules from molecular dynamics simulations," ACS Nano **9**, 8255–8268 (2015).

[23]E. Bordes, J. Szala-Bilnik, and A. H. Padua, "Exfoliation of graphene and fluorographene in molecular and ionic liquids," Faraday Discuss. **206**, 61–75 (2018).

[24]S. Plimpton, "Fast parallel algorithms for short-range molecular-dynamics," J. Comput. Phys. **117**, 1–19 (1995).

[25]S. J. Stuart, A. B. Tutein, J. A. Harrison, and I. Introduction, "A reactive potential for hydrocarbons with intermolecular interactions," J. Chem. Phys. **112**, 6472–6486 (2000).

[26]J. L. Abascal and C. Vega, "A general purpose model for the condensed phases of water: TIP4P/2005," J. Chem. Phys. **123**, 234505 (2005).

[27]N. Schmid, A. P. Eichenberger, A. Choutko, S. Riniker, M. Winger, A. E. Mark, and W. F. Van Gunsteren, "Definition and testing of the GROMOS force-field versions 54A7 and 54B7," Eur. Biophys. J. **40**, 843–856 (2011).

[28]A. K. Malde, L. Zuo, M. Breeze, M. Stroet, D. Poger, P. C. Nair, C. Oostenbrink, and A. E. Mark, "An automated force field topology builder (ATB) and repository: Version 1.0," J. Chem. Theory Comput. **7**, 4026–4037 (2011).

[29]S. Nose, "A molecular dynamics method for simulations in the canonical ensemble," Mol. Phys. **52**, 255–268 (1984).

[30]W. G. Hoover, "Canonical dynamics: Equilibrium phase-space distributions," Phys. Rev. A **31**, 1695–1697 (1985).

[31]M. A. González and J. L. F. Abascal, "The shear viscosity of rigid water models," J. Chem. Phys. **132**, 096101 (2010).

[32]A. Henni, J. J. Hromek, P. Tontiwachwuthikul, and A. Chakma, "Volumetric properties and viscosities for aqueous N-Methyl-2-pyrrolidone solutions from 25 °C to 70 °C," J. Chem. Eng. Data **49**, 231–234 (2004).

[33]D. J. Henry, C. A. Lukey, E. Evans, and I. Yarovsky, "Theoretical study of adhesion between graphite, polyester and silica surfaces," Mol. Simul. **31**, 449–455 (2005).

[34]A. Ferguson and E. J. Irons, "On surface energy and surface entropy," Proc. Phys. Soc. **53**, 182–185 (1941).

[35]A. B. López, A. García-Abuín, D. Gómez-Díaz, M. D. La Rubia, and J. M. Navaza, "Density, speed of sound, viscosity, refractive index and surface tension of N-methyl-2-pyrrolidone + diethanolamine (or triethanolamine) from T = (293.15 to 323.15) K," J. Chem. Thermodyn. **61**, 1–6 (2013).

[36]J. Alejandre and G. A. Chapela, "The surface tension of TIP4P/2005 water model using the Ewald sums for the dispersion interactions," J. Chem. Phys. **132**, 014701 (2010).

[37]S. K. Kannam, B. D. Todd, J. S. Hansen, and P. J. Daivis, "How fast does water flow in carbon nanotubes ?," J. Chem. Phys. **138**, 094701 (2013).

[38]E. Lauga, M. Brenner, and H. Stone, *Microfluidics: The No-Slip Boundary Condition*, Springer Handbook of Experimental Fluid Mechanics (Springer, 2007), pp. 1219–1240.

[39]L. Bocquet and J. L. Barrat, "Flow boundary conditions from nano- to microscales," Soft Matter **3**, 685–693 (2006).

[40]C. Pozrikidis, *Boundary Integral and Singularity Methods for Linearized Viscous Flow* (Cambridge University Press, Cambridge, 1992).

[41]C. Kamal, S. Gravelle, and L. Botto, "Graphene nanoplatelets attain a stable orientation in a shear flow" (unpublished).

[42]A. Maali, T. Cohen-bouhacina, and H. Kellay, "Measurement of the slip length of water flow on graphite surface," Appl. Phys. Lett. **92**, 053101 (2008).

[43]D. Ortiz-Young, H.-C. Chiu, S. Kim, K. Voïtchovsky, and E. Riedo, "The interplay between apparent viscosity and wettability in nanoconfined water," Nat. Commun. **4**, 2482 (2013).

[44]G. Tocci, L. Joly, and A. Michaelides, "Friction of water on graphene and hexagonal BN from *ab initio* methods: Very different slippage despite very similar interface structures," Nano Lett. **14**, 6872–6877 (2014).

[45]J. Shen, Y. He, J. Wu, C. Gao, K. Keyshar, X. Zhang, Y. Yang, M. Ye, R. Vajtai, J. Lou, and P. M. Ajayan, "Liquid phase exfoliation of two-dimensional materials by directly probing and Matching surface tension components," Nano Lett. **15**, 5449–5454 (2015).

[46]J. G. Kirkwood and F. P. Buff, "The statistical mechanical theory of surface tension," J. Chem. Phys. **17**, 338–343 (1949).

[47]T. Dreher, C. Lemarchand, L. Soulard, E. Bourasseau, P. Malfreyt, and N. Pineau, "Calculation of a solid/liquid surface tension: A methodological study," J. Chem. Phys. **148**, 034702 (2018).

[48]T. Dreher, C. Lemarchand, N. Pineau, E. Bourasseau, A. Ghoufi, and P. Malfreyt, "Calculation of the interfacial tension of the graphene-water interaction by molecular simulations," J. Chem. Phys. **150**, 014703 (2019).

[49]P. G. Karagiannidis, S. A. Hodge, L. Lombardi, F. Tomarchio, N. Decorde, S. Milana, I. Goykhman, Y. Su, S. V. Mesite, D. N. Johnstone, R. K. Leary, P. A. Midgley, N. M. Pugno, F. Torrisi, and A. C. Ferrari, "Microfluidization of graphite and formulation of graphene-based conductive inks," ACS Nano **11**, 2742–2755 (2017).

[50] P. Poulin, R. Jalili, W. Neri, F. Nallet, T. Divoux, A. Colin, S. H. Aboutalebi, G. Wallace, and C. Zakri, "Superflexibility of graphene oxide," Proc. Natl. Acad. Sci. U. S. A. **113**, 11088 (2016).

[51] P. S. Lingard and R. L. Whitmore, "The deformation of disc-shaped particles by a shearing fluid with application to the red blood cell," J. Colloid Interface Sci. **49**, 119–127 (1974).

[52] L. Botto, "Towards nanomechanical models of liquid-phase exfoliation of layered 2D nanomaterials: Analysis of a pi-peel model," Front. Mater. **6**, 302 (2019).

[53] G. Salussolia, N. Pugno, E. Barbieri, and L. Botto, "Micromechanics of liquid-phase exfoliation of a layered 2D material: A hydrodynamic peeling model," J. Mech. Phys. Solids **134**, 103764 (2019).